The 2010 IEEE/RSJ International Conference on
Intelligent Robots and Systems
October 18-22, 2010, Taipei, Taiwan

Addressing Input Saturation and Kinematic Constraints of Overactuated Undercarriages by Predictive Potential Fields

Christian P. Connette, Andreas Pott, Martin Hägele, Alexander Verl

Abstract— **Currently, pseudo-omnidirectional, wheeled mobile robots with independently steered and driven wheels seem to provide a solid compromise between complexity, flexibility and robustness. Yet, such undercarriages are imposed to the risk of actuator fighting and suffer from singular regions within their configuration space.**

To address these problems we expand a previously developed potential field (PF) based approach by expanding it with a predictive horizon. The proposed method is based on a model predictive control (MPC) approach, incorporating a gradient descent optimization step via the Pontryagin minimum principle. To enforce adherence to the constraints during optimization, we modify the Lagrange-multipliers within the backpropagation of the costates. The proposed approach is evaluated simulatively w.r.t. the undercarriage of the Care-O-bot® 3 mobile robot and is compared to the potential field based and a model predictive control approach.

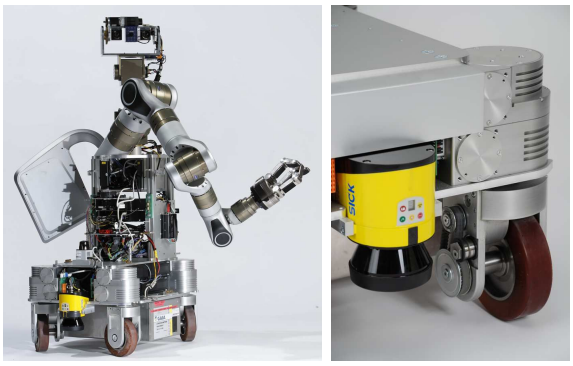

Fig. 1. Care-O-bot® 3, without coating. To allow quasi-omnidirectional motion the mobile base is composed by four actively steered and driven wheels (www.care-o-bot-research.org).

I. Introduction

Future service robot applications will impose high requirements on the employed mobility concepts [1]. Lately, pseudo-omnidirectional, wheeled mobile robots whose undercarriage is composed by independently steerable and drivable wheels [2], [3], [4], have emerged as an intermediate term solution. Such systems present a viable compromise between complexity, robustness and flexibility.

According to the work by Campion et al. [5], such robots have 3 degrees-of-freedom (DoF). These DoF are split into the degree of steerability $\delta_s = 2$, associated to the number of independently steerable wheels, and the degree of mobility $\delta_m = 1$, associated to the instantaneously accessible velocity space for the planar motion. Thus, pseudo-omnidirectional mobile robots are able to realize arbitrary velocity and rotational commands, however only after reorienting its wheels. Furthermore, this means that such systems are often overactuated [6]. Therefore, it is important to precisely coordinate all motions to reduce actuator fighting [7], [8]. Moreover, such pseudo-omnidirectional, wheeled mobile robots suffer from singular regions within their configuration space [9], [10], [11]. One possibility to solve this problem [9], [10] is to take into account the singular regions already during trajectory planning and to constrain the accessible velocity space of the robot to a region without singular configurations. Another approach [11] is to avoid singular configurations by treating them as obstacles in a navigation problem and implementing a Potential Field (PF) [12], [13] based controller.

This work was conducted in the department of Robot Systems at the Fraunhofer Institute for Manufacturing Engineering and Automation (IPA), 70569 Stuttgart, Germany; Contact: phone: +49 711 970 1325; e-mail: christian.connette@ipa.fraunhofer.de

Yet, while successfully applied to various navigation problems [14], [15], [16], PF's are known for some drawbacks. For instance PF's are sensitive to local minima. Moreover, when applied to systems changing fast compared to their sample time, PF approaches may lead to local oscillations [17]. Introducing a predictive horizon – according to the methodologies developed within the model predictive control (MPC) domain [18], [19] – promises to remedy the last mentioned problem. While originally focusing on systems with slow dynamics there exists meanwhile a series of works applying MPC approaches to the field of mobile robot navigation. Several works [20], [21], [22] motivated the objective function via repulsive potential fields.

Within this work, a potential field approach with a predictive horizon is derived and applied to the control of a pseudo-omnidirectional mobile robot. To address the interconnected problems of non-holonomic constraints and actuator concurrency control is performed within the spherical representation of the ICM space. To motivate the introduction of a predictive horizon, we draw from the methodologies developed in the MPC domain. Therefore, we start from gradient descent based optimization of the objective function via the Pontryagin minimum principle (PMP) [20], [22]. Then, constraints on the system velocity are enforced by modifying the costates during backpropagation. Therefore, the analogy between Lagrange-multipliers and forces is exploited. Moreover, the calculation of equilibrium velocities, where frictional and attractive forces cancel out each other [12], is expanded to take into account also repulsive forces. The algorithm is evaluated in simulation and compared to the earlier implemented PF- and a MPC-approach.

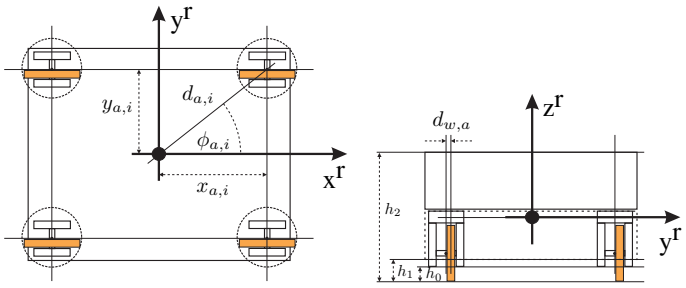

Fig. 2. Top and front view of Care-O-bot® 3's mobile base

II. Problem Formulation

A. System Architecture

The platform (Fig. 1 and Fig. 2) has a rectangular shape with a length of approximately 60 cm and a width of about 50 cm. The steering-axes of the wheels lie at $x_{a,i} = \pm 23{,}5$ cm and $y_{a,i} = \pm 18{,}5$ cm. The wheels are sidewards off-centered to the steering-axes by $d_{w,a} = 2{,}2$ cm. The chassis clearance h_1 is about 5 cm. The total height of the system h_2 is approximately 35 cm.

Current and velocity control for the actuators is provided by off-the-shelf motor controllers. The lowest software-layer comprises the control loop for the robot velocities (v_x, v_y, ω) generating the set point values $(\vec{\varphi}_s, \dot{\vec{\varphi}}_d)$ for all motor controllers. It provides an interface for higher level components, for instance, a user interface such as a joypad (Fig. 3(a)), the navigation module (Fig. 3(b)) which closes the position loop or the arm-control module (Fig. 3(c)) sending velocity requests to the platform. Therefore, the velocity control loop has to:

1) ensure adherence to the non-holonomic constraints
   a) identify the valid configuration $(\vec{\varphi}_s, \dot{\vec{\varphi}}_d)$
   b) derive a valid trajectory $(\vec{\varphi}_s, \dot{\vec{\varphi}}_s, \dot{\vec{\varphi}}_d, \ddot{\vec{\varphi}}_d)$
   c) respect the actuator limits $(\vec{\varphi}_{s,u}, \dot{\vec{\varphi}}_{d,u})$
2) approach the commanded velocities fast
3) compensate the steer/drive-coupling

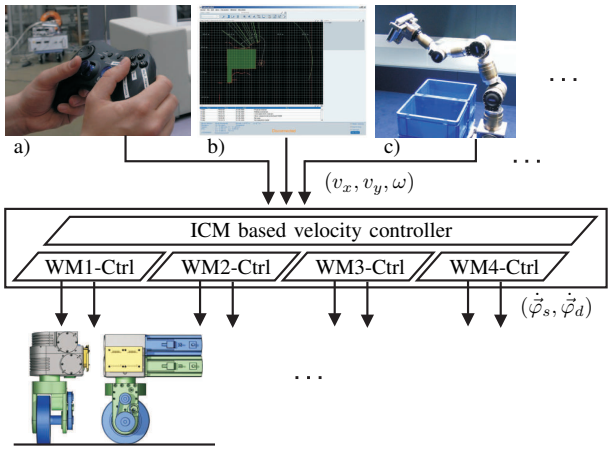

Fig. 3. Schematic of Care-O-bot® 3's software-structure. The ICM based velocity controller synchronizes the motion of all wheels. The WMx-controllers synchronize the steer and drive motors of the single wheels.

B. State-Space Representation

To decouple the control of the undercarriage from the trajectory-control and to provide a simple interface for commanding velocities, the state-space of the undercarriage is reduced to the velocities in the robot coordinate system. The current state of motion $\vec{t}_r$ then becomes a function

$$\vec{t}_r = \vec{g}(\vec{\varphi}_s, \dot{\vec{\varphi}}_d) \tag{1}$$

of the directions $\vec{\varphi}_s$ and the rotations $\dot{\vec{\varphi}}_d$ of all wheels. Within this work, we focus on a kinematic description of the undercarriage and therefore omit the calculation of wheel-ground contact forces. As a result we have to take into account the non-holonomic constraints of each wheel resulting in eight additional constraints P. According to [5] this results in a system with 3 DoF, from which two are associated to the configuration space of the system $\delta_s = 2$ and one is associated to its motion space $\delta_m = 1$. Based on [5] and [9] we motivated in [23] that one possible state representation of the combined motion and configuration space of such a system is the spherical coordinate transform of its twist-vector

$$\vec{t}_r = \begin{pmatrix} \rho_r \\ \varphi_r \\ \theta_r \end{pmatrix} = \begin{pmatrix} \sqrt{v_{x,r}^2 + v_{y,r}^2 + (\omega_r \cdot d_{max})^2} \\ \arctan_2\left(\frac{v_{r,y}}{v_{r,x}}\right) \\ \arctan\left(\frac{\omega_r \cdot d_{max}}{\sqrt{v_{r,x}^2 + v_{r,y}^2}}\right) \end{pmatrix}, \tag{2}$$

where $v_{x,r}$ and $v_{y,r}$ are the robot's linear velocities in the robot coordinate system, ω_r its rotational velocity and d_{max} a norming factor. Hence, the kinematics equations can be reformulated to calculate steering angles and rotational rates as a function of the spherical twist vector.

$$\left(\vec{\varphi}_s, \dot{\vec{\varphi}}_d\right)^T = \vec{f}_{\vec{k}_1, \vec{k}_2}\left(\rho_r, \varphi_r, \theta_r\right) \tag{3}$$

$$\left(\dot{\vec{\varphi}}_s, \ddot{\vec{\varphi}}_d\right)^T = \nabla \vec{f}_{\vec{k}_1, \vec{k}_2} \cdot \left(\dot{\rho}_r, \dot{\varphi}_r, \dot{\theta}_r\right)^T, \tag{4}$$

where $\vec{k}_1$ and $\vec{k}_2$ are parameters characterizing the configuration of the undercarriage during startup.

C. Input Saturation and State Constraints

This state-space representation and the according inverse kinematics equations become singular, when the instantaneous centre of motion (ICM) passes through one of the steering axis. In effect, the steering velocity of a wheel grows unbounded, as the ICM moves close to that wheel (Fig. 4). However, due to the non-holonomic constraints of the system it is unfeasible to simply constrain the commanded steering velocities $\dot{\vec{\varphi}}_s$ to their maximum values. Doing so destroys the synchronicity of the wheels and leads to actuator conflicts, causing unsteady motions or damaging the actuators.

In [11] a potential-field based controller was applied to avoid the critical regions by representing them as repulsive potentials. However, due to the limited time resolution problems such as oscillations in the vicinity of the repulsive potentials were encountered. The introduction of a predictive horizon, which can be motivated through the MPC formalism, has the potential to remedy these problems.

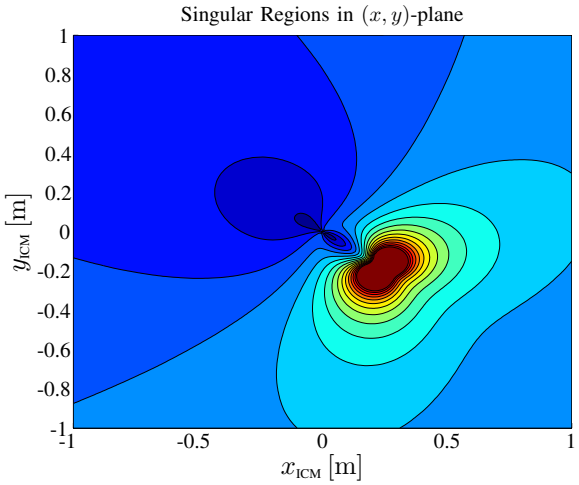

(a) Steering velocities with respect to position of ICM in cart. space

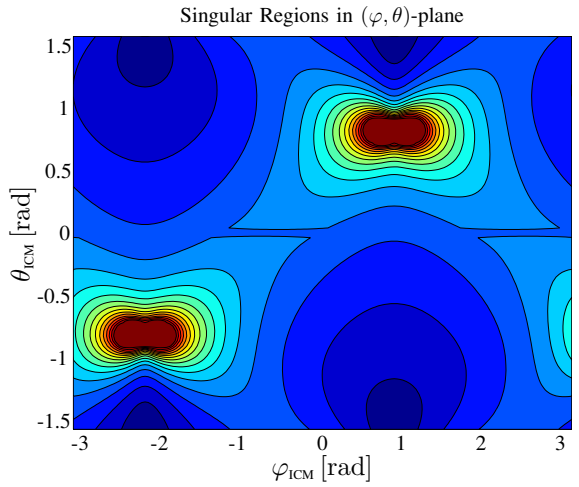

(b) Steering velocities with respect to position of ICM in spher. space

Fig. 4. Worst case approximation for necessary steering velocity for an ICM motion with constant absolute speed of 1.5π rad/s. Dark red spaces indicate regions where the necessary steering velocity grows bigger than 8π rad/s, which is the maximum allowed steering rate for a wheel-module.

III. Model Predictive Control

A. General Approach

The idea of model predictive control is to solve an optimal control problem for a system

$$\dot{\vec{x}} = A\vec{x} + B\vec{u} \ , \tag{5}$$

where $\vec{x}$ is the vector of system sates, $\vec{u}$ are the input variables, A the matrix representing the system dynamics and B is representing the influence of the input variables on the system. The MPC approach then derives the input $\vec{u}$ such that it optimizes the objective function

$$J = \phi(\vec{x}(T)) + \int_{t=0}^{T} \mathcal{L}(\vec{x}, \vec{u}, t)dt \tag{6}$$

over a finite time horizon T, by predicting the future development of the system. In this context $\phi(x(T))$ penalizes a deviation of goal state and predicted end state and $\mathcal{L}$ is the Langrangian of the system. For discrete time systems the integral in (6) is replaced by a sum over the timesteps until the prediction horizon. A straight forward choice for $\mathcal{L}$ is

$$\mathcal{L} = J^z + J^u \ , \tag{7}$$

$$J^z = 1/2 \cdot (\vec{x}_{cmd}(t) - \vec{x}(t))^T Q(\vec{x}_{cmd}(t) - \vec{x}(t)), \tag{8}$$

$$J^u = 1/2 \cdot \vec{u}(t)^T R\vec{u}(t) \ , \tag{9}$$

where R and Q are both positive semidefinit diagonal matrices. Thus, the deviation of the current or predicted state $\vec{x}(t)$ from the target state $\vec{x}_{cmd}(t)$ along the trajectory are penalized, as well as the applied control effort J^u. The advantage of model predictive control is, that it is straight forward to take into account state constraints or input saturation when calculating the optimal input $\vec{u}$. Therefore, it is possible to address the singularities mentioned in section II-C by incorporating them via the Langrangian $\mathcal{L}$ (section IV-A) into the objective function.

B. Optimization by Gradient Descent

One possible method to perform the optimization step is gradient descent based optimization by the Pontryagin minimum principle (PMP) [20], [22]. The basic idea of the PMP is to minimize the Hamiltonian

$$\mathcal{H}(\vec{x}, \vec{u}, \vec{\lambda}, t) = \mathcal{L}(\vec{x}, \vec{u}, t) + \vec{\lambda}^T(t)\vec{f}(\vec{x}, \vec{u}) \tag{10}$$

which incorporates the objective functional J through the Lagrangian and the system dynamics $\vec{f}(\vec{x}, \vec{u})$ via the costates or Lagrange-multipliers $\vec{\lambda}$. As the approach is not constrained to linear systems the dynamics is expressed by the function $\vec{f}(\vec{x}, \vec{u})$ instead of using equation (5). One prerequisite for obtaining an optimal solutions is that the Hamiltonian $\mathcal{H}$ and thus the objective function J has to be continously differentiable. Then a solution optimizes the problem if the conditions

$$\dot{\vec{x}} = {}^{\partial\mathcal{H}}/_{\partial\vec{\lambda}} \ , \tag{11}$$

$$\dot{\vec{\lambda}} = -{}^{\partial\mathcal{H}}/_{\partial\vec{x}} \ , \text{ with} \tag{12}$$

$$\vec{\lambda}(T) = \frac{\partial\phi(\vec{x}(T))}{\partial\vec{x}} \text{ and} \tag{13}$$

$${}^{\partial\mathcal{H}}/_{\partial\vec{u}} = 0 \tag{14}$$

are fullfilled. It has to be noted that equation (14) is not applicable if $\vec{u}$ is constrained to an intervall with optimal $\vec{u}_{opt}$ at the edges or outside this intervall. Optimization in discrete time is performed analogously, while the Hamiltonian

$$\mathcal{H}(\vec{x}_k, \vec{u}_k, \vec{\lambda}_k, k) = \mathcal{L}(\vec{x}_k, \vec{u}_k, k) + \vec{\lambda}_{k+1}^T\vec{f}(\vec{x}_k, \vec{u}_k) \tag{15}$$

then depends on the costate $\vec{\lambda}_{k+1}$ from the next time step. An explicit formulation of the optimization procedure when embedded into a MPC approach can be found in [20], [22]. Employing the PMP for optimization is especially appropriate, as the gradient descent has analogies to theoretical mechanics and thus fits especially well to the earlier implemented PF approach.

IV. Predictive Potential Fields

A. Specifying Dynamics and Objective Function

To ensure adherence to the non-holonomic constraints the system state is composed by the spherical coordinates of the twist vector, as described in equation (2). Choosing this state representation the transformation into the according steering angles and drive rates as given in equation (3) becomes nonlinear. Thus, the resulting commanded steering velocities $\dot{\vec{\varphi}}_S$ are a function of both, the command inputs $(\dot{\rho}_r, \dot{\varphi}_r, \dot{\theta}_r)^T$ as well as the current state $(\rho_r, \varphi_r, \theta_r)$. Therefore and to achieve smooth control inputs, the state vector is augmented by adding an additional integration step and by choosing B in equation (5) such that only the augmented states $(\dot{\rho}_r, \dot{\varphi}_r, \dot{\theta}_r)^T$ are directly controlled through the inputs $\vec{u}_k$. To allow shorter formulation the states $(\rho_r, \dot{\rho}_r)^T$ are omitted in the following. These states do not influence the critical steering commands. Hence, the vector $\vec{x}_r$ representing the system state of the pseudo-omnidirectional undercarriage and the input-vector $\vec{u}_r$ are set to

$$\vec{x}_r = \left(\varphi_r, \theta_r, \dot{\varphi}_r, \dot{\theta}_r\right)^T , \tag{16}$$

$$\vec{u}_r = \left(F_{\varphi,r}, F_{\theta,r}\right)^T \tag{17}$$

and the system dynamics become

$$\vec{f}(\vec{x}, \vec{u}) = \left(x_3, x_4, {}^{u_1}/_m, {}^{u_2}/_m\right)^T \text{ , with} \tag{18}$$

$$A = {}^{\partial \vec{f}}/_{\partial \vec{x}} , \tag{19}$$

$$B = {}^{\partial \vec{f}}/_{\partial \vec{u}} . \tag{20}$$

The introductiuon of the integration constant m in equation (18) was chosen to stick to the analogy of the input $\vec{u}$ to virtual forces $(F_{\varphi,r}, F_{\theta,r})^T$. For a convenient writing it is following assumed that $m = 1$ and the integration constant is omitted.

Thus, saturation of the steering actuator inputs can be avoided by formulation of a state constraint on the augmented state-space. Therefore, the critical regions are incorporated into the fitness criteria in form of repulsive potentials

$$J = \phi(x_N) + \sum_{k=0}^{N-1} \left(J^z + J^u + \sum_{i=0}^{M} J_i^o \right) \tag{21}$$

$$J_i^o = \begin{cases} \mu^o \left(\frac{1}{r_i} - \frac{1}{r_0}\right)^2 & \forall \quad r_i \le r_0 \\ 0 & \forall \quad r_i > r_0 \end{cases} \tag{22}$$

$$r_i = \sqrt{\left(\frac{\varphi_r - \varphi_i^o}{a}\right)^2 + \left(\frac{\theta_r - \theta_i^o}{b}\right)^2}, \tag{23}$$

where M is the number of steerable wheels, μ^o is a scaling factor to adjust the gradient of the repulsive potentials, r_0 constrains the region of influence of the potential fields and $(\varphi, \theta)_i^o$ is the position of the i-th wheel's steering axis after transformation into the spherical twist coordinate space. To continue with the analogy to forces and potential fields, the derivatives $(\dot{\varphi}_{r,cmd}, \dot{\theta}_{r,cmd})$ along the commanded state trajectory are set to $\vec{0}$ by default. Accordingly, the diagonal elements of Q associated to the derivatives of the original states are set to

$$q_{33} = q_{44} = k_\nu , \tag{24}$$

resembling friction coefficients while the diagonal elements associated to the original state variables are set to

$$q_{11} = q_{22} = k_p \tag{25}$$

resembling a proportional spring coefficient. Therefore, our system and objective function is analogous to a mechanical system subject to attractive, repulsive and dissipative forces.

B. Costate Enforcement

The so far proposed control scheme can be inadequate if the state shows a large control difference in the original states $(x_{r,1}, x_{r,2})^T$. As all states enter the objective function quadratic, this can result in control-inputs which lead to high velocities $(x_{r,3}, x_{r,4})^T$. However, increasing k_ν to penalize high velocities leads to a slow system response. One possibility to cope with this is to define an additional penalty J^{z*} wich only penalizes $(x_{r,3}, x_{r,4})^T$ with a high value k_ν^*, that is only taken into account when $(x_{r,3}, x_{r,4})^T$ exceed a certain limit. For a more cenvenient writing we write $\vec{v}_r$ instead of $(x_{r,3}, x_{r,4})^T$ in the following. One drawback of this approach is, that high gains usually tend to adversely influence stability and convergence. Moreover, this measure is only effective when the velocity has already reached a high value.

An alternative was sketched by Khatib in his potential field approach [12]. With respect to velocity servo-control he proposed to calculate an equilibrium velocity

$$\vec{v}_{eq} = {}^{k_p}/_{k_\nu} \cdot (\vec{x}_{cmd} - \vec{x}) , \tag{26}$$

where attractive and frictional forces would cancel out each other. This velocity is then compared with the maximum allowed velocity v_{max}. The smaller one is chosen and the forces associated to the attractive potential are calculated based on the deviation of the system's current velocity from this equilibrium velocity

$$F_{att} = k_\nu (\min\left(1, \frac{v_{max}}{|\vec{v}_{eq}|}\right) \cdot \vec{v}_{eq} - \vec{v}_r) . \tag{27}$$

Bearing in mind the analogies of the Hamiltonian used in mathmatical optimization and the Hamiltonian as defined in theoretical mechanics we propose to transfer the approach of Khatib to the calculation of the costates. In mechanics the Hamiltonian $\mathcal{H}^*$ resembles the total energy of the system

$$\mathcal{H}^* = \sum_i \vec{p}_i \dot{\vec{q}}_i - \mathcal{L}^* \tag{28}$$

where $\dot{\vec{q}}_i$ are the generalized coordinates of the system, $\vec{p}_i$ are the generalized momenta or the impulses respectively and $\mathcal{L}^*$ is the Langrangian as defined in mechanics. The evolution of the system is then governed by the two canonical equations

$$\dot{\vec{p}} = -{}^{\partial \mathcal{H}^*}/_{\partial \vec{q}} , \tag{29}$$

$$\dot{\vec{q}} = {}^{\partial \mathcal{H}^*}/_{\partial \vec{p}} . \tag{30}$$

Comparing equation (29) and equation (12) of the PMP optimization and bearing in mind that the derivative of an impulse $\dot{\vec{p}}$ is a force, illustrates the analogy between the derivative of the costate $\dot{\vec{\lambda}}$ and forces. Writing out equation (12) and equation (14) one obtains

$$\frac{\partial \mathcal{H}}{\partial \vec{u}} = \vec{u}^T R + \vec{\lambda}^T \frac{\partial \vec{f}(\vec{x},\vec{u})}{\partial \vec{u}} , \quad (31)$$

$$\dot{\vec{\lambda}}^T = \underbrace{(\Delta \vec{x}_r)^T Q - \sum_{i=0}^{M} \frac{\partial J_i^o}{\partial \vec{x}}}_{-\partial \mathcal{L}/\partial \vec{x}_k = \dot{\vec{\lambda}}^T} - \underbrace{\vec{\lambda}^T \frac{\partial \vec{f}(\vec{x},\vec{u})}{\partial \vec{x}}}_{:\approx \vec{v}_{r,p} k_{nu}} , \quad (32)$$

where $\Delta \vec{x}_r$ is the control difference $\vec{x}_{r,cmd} - \vec{x}_r$ and $\vec{v}_{r,p}$ is a pseudo-velocity resulting from pure integration of the proportional forces on the original states. The first underbraced term is the negative derivative of the Lagrangian $\mathcal{L}$ and thus resembles the negative of the forces originated by the potential fields and the frictional coefficients

$$\dot{\lambda}_{\mathcal{L}1} = (\varphi_{r,cmd} - \varphi_r) q_{11} - \sum_{i=0}^{M} \frac{\partial J_i^o}{\partial \varphi_r} \quad (33)$$

$$\dot{\lambda}_{\mathcal{L}2} = (\theta_{r,cmd} - \theta_r) q_{22} - \sum_{i=0}^{M} \frac{\partial J_i^o}{\partial \theta_r} \quad (34)$$

$$\dot{\lambda}_{\mathcal{L}3} = (\dot{\varphi}_{r,cmd} - \dot{\varphi}_r) q_{33} \quad (35)$$

$$\dot{\lambda}_{\mathcal{L}4} = (\dot{\theta}_{r,cmd} - \dot{\theta}_r) q_{44} , \quad (36)$$

with $\dot{\varphi}_{r,cmd} \equiv \dot{\theta}_{r,cmd} \equiv 0$ by default, as mentioned in section IV-A.

In analogy to [12] the pseudo-velocities $\vec{v}_{r,p}$ can be interpreted as specifying a desired velocity in a velocity servo-control. Having in mind the system dynamics as defined in equation (18) one can see that the evolution of the input $\vec{u}$ in equation (31) is directly only influenced by the costates (λ_3, λ_4) associated to the velocities $\vec{v}_r$. Thus, to ensure that the controller enforces a limit v_{max} even if the control-difference in the original state is large we calculate an equilibrium velocity according to

$$\dot{\varphi}_{eq} = {}^1\!/_{q_{33}} \cdot \left(-q_{11}(\varphi_{r,cmd} - \varphi_r) + \sum_{i=0}^{M} \frac{\partial J_i^o}{\partial \varphi_r} \right) \quad (37)$$

$$\dot{\theta}_{eq} = {}^1\!/_{q_{44}} \cdot \left(-q_{22}(\theta_{r,cmd} - \theta_r) + \sum_{i=0}^{M} \frac{\partial J_i^o}{\partial \theta_r} \right) \quad (38)$$

$$|\vec{v}_{eq}| = \sqrt{\varphi_{eq}^2 + \theta_{eq}^2} \quad (39)$$

and redefine the derivated Lagrangian from equation (32)

$$\dot{\lambda}_{\mathcal{L}1} := 0 \quad (40)$$

$$\dot{\lambda}_{\mathcal{L}2} := 0 \quad (41)$$

$$\dot{\lambda}_{\mathcal{L}3} := \left(\min\left(1, \frac{v_{max}}{|\vec{v}_{eq}|}\right) \cdot \dot{\varphi}_{eq} - \dot{\varphi}_r \right) q_{33} \quad (42)$$

$$\dot{\lambda}_{\mathcal{L}4} := \left(\min\left(1, \frac{v_{max}}{|\vec{v}_{eq}|}\right) \cdot \dot{\theta}_{eq} - \dot{\theta}_r \right) q_{44} . \quad (43)$$

V. Results

A. Simulative Results

The proposed approach is evaluated in simulation with respect to the specific kinematics of Care-O-bot® 3. The system is simulated with a time step size of 20 ms. The simulation takes into account a transport delay of the measured sizes of 10 ms and the restrictions on velocity and acceleration of the wheel modules.

The simulation was done for three different controllers: for the earlier implemented conventional potential field based controller (dotted black lines in Fig. 5), for a classical model predictive control approach with an additional penalty $J^* = (\max(0, (\dot{x}_{max} - |\dot{x}_{eq}|)\, k^*_{nu}))^2$ (dash-dotted blue) and the proposed predictive potential field (solid green) which is based on enforcing the costates during the MPC optimization step. To simplify comparison of the results all controllers were tuned to be similar fast.

Fig. 5 depicts the results of a simulation run for a sequence of target configurations, that leads to critical situations for the system configuration. One can see that the conventional potential field based approach is clearly outperformed by the two predictive approaches. Its trajectory shows strong oscillations when running into the repulsive potentials (Fig. 5(a)). While being quite fast for the first two sections (a to b; b to c) of the trajectory these oscillations result in increased duration for the last section (Fig. 5(b)). Moreover, the PF approach causes significantly larger steering rate commands, exceeding the limits of the system (Fig. 5(c)). Of course the PF controller can be tuned to show stable behavior with less oscillations and lower steering rates. However, this results in a significantly slower control performance.

The two MPC based approaches show similar results. Yet, one can see that, while the path of the classical MPC approach is slightly smoother than that of the approach with predictive potential fields (Fig. 5(a)), the last one is faster especially in the first two sections (Fig. 5(b)) and goes with smaller maximum steering rates. Moreover, during implementation the proposed approach with enforcing the costates has proven to be more robust to parameter changes than the conventional MPC approach. One reason for that might be, that by constraining the equilibrium velocity and modifying the costates, the inputs stay smaller, even when the trajectory bumps into a repulsive potential. Thus, especially the optimization step width could be set to a higher value.

B. Experimental Results

The proposed controller with predictive potential fields was implemented and tested on the mobile base of Care-O-bot® 3. The controller was run on a MacBook Pro with 2.4Ghz Intel Core2Duo Processor. The processing of one control step (prediction horizon $N_p = 32$, number of iterations $N_i = 4$) took about 5.5 ms. Fig. 6 depicts the behaviour of the controller for an arbitrary trajectory commanded manually using a joystick. The experimental results support the simulation results. The controller avoids the critical regions following a smooth trajectory and keeps the steering rate bounded.

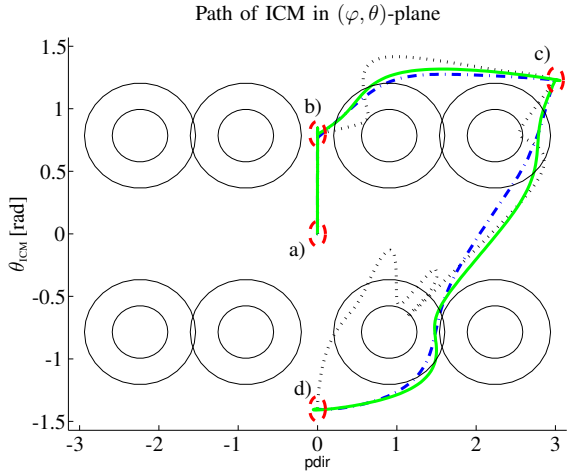

(a) Resulting paths of ICM in the (φ,θ)-plane for different controllers

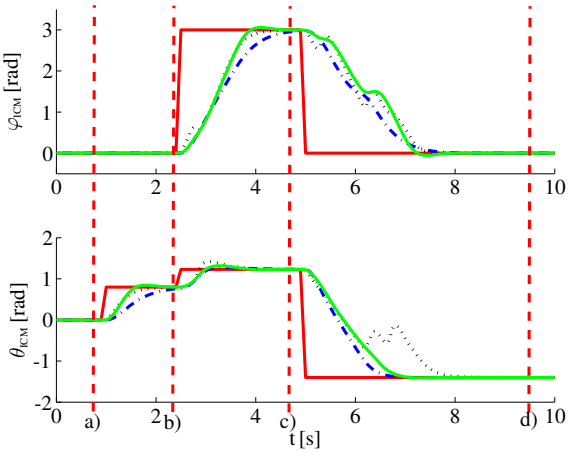

(b) Set point values (red solid) and resulting controlled values of (ρ,φ,θ)

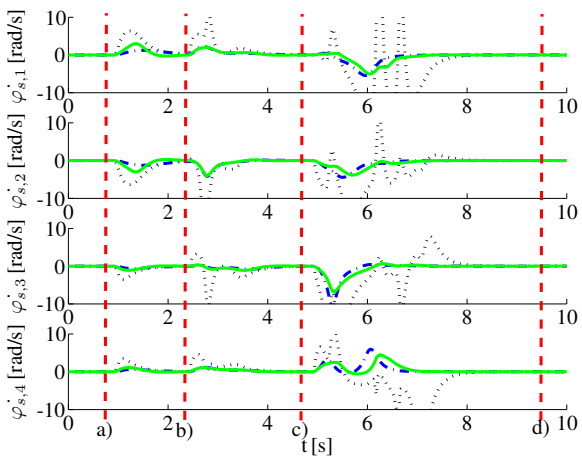

(c) Resulting wheel steering rates in all wheels

Fig. 5. Simulation Results: ICM path in the (φ,θ)-plane for the following sequence of four target configurations (a) $(\varphi,\theta) = (0,0)$; b) $(\varphi,\theta) = (0,0.8)$; c) $(\varphi,\theta) = (3,1.23)$; d) $(\varphi,\theta) = (0,-1.4)$) and a maximum velocity $|\dot{x}_{eq}| = 1\pi\,\mathrm{rad/s}$. The target configurations are indicated with red dashed lines. Results are depicted for the three investigated controllers: conventionell potential ield (dotted black), classical model predictive controller (dash-dotted blue) and controler with enforced costates (solid green).

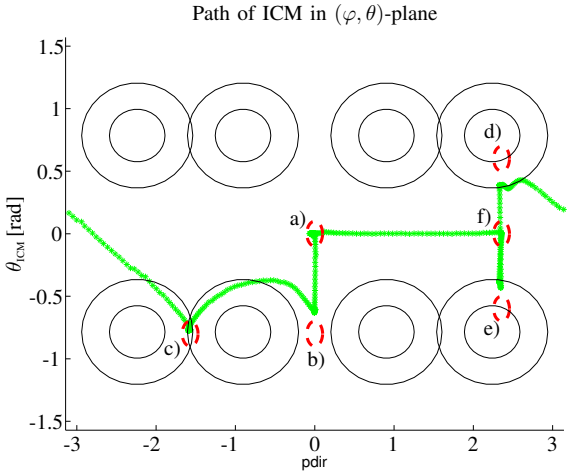

(a) Resulting paths of ICM in the (φ,θ)-plane for different controllers

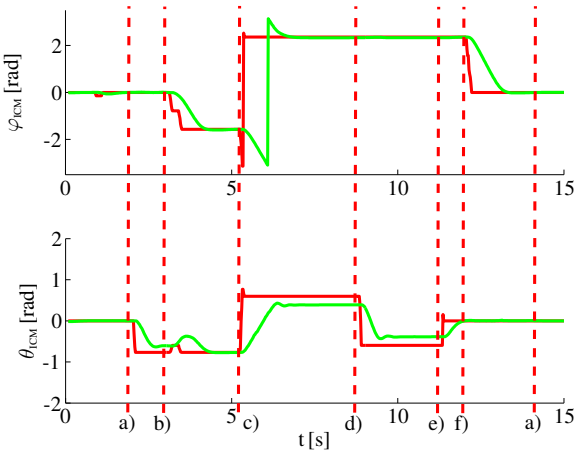

(b) Set point values (red solid) and resulting controlled values of (ρ,φ,θ)

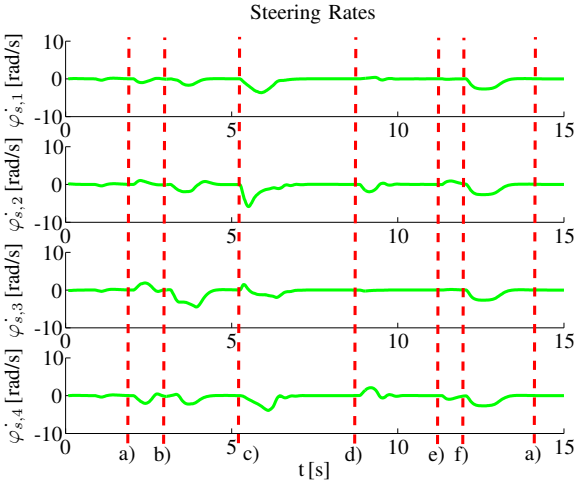

(c) Resulting wheel steering rates in all wheels

Fig. 6. Experimental Results: Resulting ICM path in the (φ,θ)-plane for a sequence of six target configurations (a, b, c, d, e, f, a). The target configurations are indicated with red dashed lines. The figure shows the results obtained with the PPF controller (solid green) implemented on Care-O-bot® 3 mobile robot. Parameterisation of the controller is identical to the simulated controller depicted in Fig. 5.

VI. Conclusion and Future Work

Within this work, we motivated how the classical potential field formalisms, with friction terms and constrained equilibrium velocities, can be expanded by a predictive horizon. Therefore, we drew from the model predictive control methodologies. Formulating the control law according to the MPC scheme, performing gradient descent based optimization over the prediction horizon according to the Pontryagin minimum principle the constrained equilibrium velocities where introduced by modifying the Lagrange-multipliers during backpropagation of the costates. Additionally, the constrained equilibrium velocities were extended to cover the attractive as well as the repulsive forces.

We applied the proposed approach to the control of a quasi-omnidirectional undercarriage subject to actuator concurrency and input saturation constraints. The approach based on predictive potential fields clearly outperformed the conventional PF approach and showed a slightly better performance than the MPC approach. Moreover, during implementation we experienced that our approach with enforced costates was less sensitive to parameter changes. Sensitivity to parameter changes can be a critical issue during implementation of model predictive controllers.

It has to be noted that our approach apperently is not strictly derived through the underlying mathmatical formalisms but motivated by some analogies. There are two significant differences between the Hamiltonian used in optimal control and that used in theoretical mechanics. Nevertheless, interpreting our modifications as calculating a series of desired velocities along a trajectory, which is then input to an according controller motivates the legitimacy of the proposed approach. Moreover, the employed system model is conceivable simple. In fact, we treated the generality of MPC approaches against simpler design and dimensioning of the controller. Yet, the derived formalism is powerful enough for many reactive navigation tasks, where wheeled mobile robots are involved.

Besides investigating the behavior of the implemented controller within the navigation architecture of Care-O-bot® 3, we currently plan to apply the derived approach in context of people following and guiding. This seems especially interesting as it implies not only to reach a certain position, but more – by taking into account the motion of surrounding people – to follow a fast changing trajectory.

References

[1] B. Graf, M. Hans, R.D. Schraft, "Care-O-bot II - Development of a Next Generation Robotic Home Assistant", *Autonomous Robots*, vol. 16, issue 2, 2004, pp 193-205.

[2] M. Fuchs, C. Borst, P. Robuffo Giordano, A. Baumann, E. Kraemer, J. Langwald, R. Gruber, N. Seitz, G. Plank, K. Kunze, R. Burger, F. Schmidt, T. Wimboeck, G. Hirzinger, "Rollin' Justin - Design Considerations and Realization of a Mobile Platform for a Humanoid Upper Body", *2009 IEEE International Conference on Robotics and Automation ICRA*, Kobe, Japan, 2009, pp 4131-4137.

[3] K.A. Wyrobek, E.H. Berger, H.F.M. van der Loos, J.K. Salisbury, "Towards a Personal Robotics Development Platform: Rationale and Design of an Intrinsically Safe Personal Robot", *2008 IEEE International Conference on Robotics and Automation ICRA*, Pasadena, USA, 2008, pp 2165-2170.

[4] U. Reiser, C.P. Connette, J. Fischer, J. Kubacki, A. Bubeck, F. Weisshardt, T. Jacobs, C. Parlitz, M. Hägele, A. Verl, "Care-O-bot 3 - Creating a product vision for service robot applications by integrating design and technology", *2009 IEEE/RSJ International Conference on Intelligent Robots and Systems IROS*, St. Louis, USA, 2009, pp 1992-1998.

[5] G. Campion, G.Bastin and B. D'Andréa-Novel, "Structural Properties and Classification of Kinematic and Dynamic Models of Wheeled Mobile Robots", *IEEE Transactions on Robotics and Automation*, vol. 12, issue 1, 1996, pp 47-62.

[6] P. Muir, C.P. Neuman, *Kinematic Modeling of Wheeled Mobile Robots*, Pittsburgh, USA, 1986

[7] R. Holmberg, O. Khatib, "Development and Control of a Holonomic Mobile Robot for Mobile Manipulation Tasks", *The International Journal of Robotics Research*, vol. 19, issue 11, 2000, pp 1066-1074.

[8] M. Lauria, I. Nadeau, P. Lepage, Y. Morin, P. Gigure, F. Gagnon, D. Ltourneau, F. Michaud, "Design and Control of a Four Steered Wheeled Mobile Robot", *IEEE 32nd Anual Conference on Industrial Electronics IECON*, Paris, France, 2006, pp 4020-4025.

[9] B. Thuilot, B. D'Andréa-Novel and A. Micaelli, "Modeling and Feedback Control of Mobile Robots Equipped with Several Steering Wheels", *IEEE Transactions on Robotics and Automation*, vol. 12, issue 3, 1996, pp 375-390.

[10] P. Robuffo Giordano, M. Fuchs, A. Albu-Schäffer, G. Hirzinger, "On the Kinematic Modelling and Control of a Mobile Platform Equipped with Steering Wheels and Movable Legs", *2009 IEEE International Conference on Robotics and Automation ICRA*, Kobe, Japan, 2009, pp 4080-4087.

[11] C.P. Connette, C. Parlitz, M. Hägele, A. Verl, "Singularity Avoidance for Over-Actuated, Pseudo-Omnidirectional, Wheeled Mobile Robots", *2009 IEEE International Conference on Robotics and Automation ICRA*, Kobe, Japan, 2009, pp 4124-4130.

[12] O. Khatib, "Real-Time Obstacle Avoidance for Manipulators and Mobile Robots", *The International Journal of Robotics Research*, vol. 5, issue 1, 1986, pp 90-98.

[13] B. Krogh, "A Generalized Potential Field Approach to Obstacle Avoidance Control", *SME Conference on Robotics Research: The Next Five Years and Beyond*, Bethlehem, USA, 1984

[14] E. Rimon, D.E. Koditschek, "Exact Robot Navigation Using Artificial Potential Functions", *IEEE Transactions on Robotics and Automation*, vol. 8, issue 5, 1992, pp 501-518.

[15] L. Chengqing, M.H. Ang Jr, H. Krishnan, L.S. Yong, "Virtual Obstacle Concept for Local-minimum-recovery in Potential-field Based Navigation", *IEEE International Conference on Robotics and Automation*, San Francisco, USA, 2000, pp 983-988.

[16] S. Shimoda, Y. Kuroda, K. Iagnemma, "Potential Field Navigation of High Speed Unmanned Ground Vehicles on Uneven Terrain", *IEEE International Conference on Robotics and Automation*, Barcelona, Spain, 2005, pp 2839-2844.

[17] Y. Koren, J. Borenstein, "Potential Field Methods and Their Inherent Limitations for Mobile Robot Navigation", *1991 IEEE International Conference on Robotics and Automation ICRA*, Sacramento, USA, pp 1398-1404.

[18] M. Morari, J.H. Lee, "Model Predictive Control: Past, Present and Future", *Computers & Chemical Engineering*, vol. 23, issue 4-5, 1999, pp 667-682.

[19] R. Findeisen, F. Allgöwer, "An Introduction to Nonlinear Model Predictive Control", *21st Benelux Meeting on Systems and Control*, Veldhoven, Netherlands, 2002, pp 1-23.

[20] W. Xi, J.S. Baras, "MPC Based Motion Control of Car-like Vehicle Swarms", *IEEE Mediterranean Conference on Control & Automation, MED '07*, Athens, Greece, 2007, pp 1-6.

[21] D.H. Shim, H.J. Kim, S. Sastry, "Decentralized Nonlinear Model Predictive Control of Multiple Flying Robots", *42nd IEEE International Conference on Decision and Control CDC*, Maui, USA, 2003, pp 3621-3626.

[22] H.J. Kim, D.H. Shim, "A flight control system for aerial robots: algorithms and experiments", *Control Engineering Practice*, vol. 11, issue 12, 2003, pp 1389-1400.

[23] C.P. Connette, A. Pott, M. Hägele, A. Verl, "Control of an Pseudo-Omnidirectional, Non-holonomic, Mobile Robot based on an ICM Representation in Spherical Coordinates", *47th IEEE Conference on Decision and Control CDC*, Cancun, Mexico, 2008, pp 4976-4983.